EUMETSAT

GSICS SEVIRI-IASI Inter-calibration Uncertainty Evaluation for Rapid Scan Service Data

Doc.No. : EUM/MET/TEN/11/0213
Issue : v1A
Date : 28 April 2011
WBS :

EUMETSAT
Eumetsat-Allee 1, D-64295 Darmstadt, Germany
Tel: +49 6151 807-7
Fax: +49 6151 807 555
http://www.eumetsat.int

Document Change Record

Issue / Revision	*Date*	*DCN. No*	*Changed Pages / Paragraphs*
1	06 April 2011		A modification of the analysis for the Meteosat data obtained in full-disc mode, which was written up as EUM/MET/TEN/09/0750
1A	29 April 2011		Minor revisions following review.

Table of Contents

1 INTRODUCTION

This document presents an analysis of the uncertainties in the GSICS inter-calibration products for the infrared channels of Meteosat/SEVIRI using Metop/IASI as a reference based on Meteosat Second Generation observations taken in Rapid Scanning Service (RSS). This is a modification of the analysis for the Meteosat data obtained in full-disc mode, which was written up as EUM/MET/TEN/09/0750. In this analysis the spatial and temporal gradients and variability have been re-assessed based on RSS data. The geometric variability term has also been revised following the relaxation of the collocation threshold for incidence angle, based on the recommendation presented in EUM/MET/TEN/09/0750.

This analysis follows the guidance provide by QA4EO [1], which is based on the Guide to the Expression of Uncertainty in Measurement (GUM) [2]. This analysis should be read in conjunction with the Algorithm Theoretical Basis Document (ATBD) [3], as the uncertainties provide *Quality Indicators* for the inter-calibration products. Together, these form part of the documentation requirements for the GSICS Procedure for Product Acceptance.

Each process of the inter-calibration algorithm is considered and the uncertainties evaluated on the key variables due to random and systematic effects. These uncertainties are then combined to produce an *error budget* giving a Type B evaluation of the combined uncertainty on the inter-calibration bias. The random component of this is then compared to the statistics of the *standard bias* (a Type A evaluation of their uncertainty) and recommendations made for adjustments of the inter-calibration algorithm to produce more consistent uncertainty estimates.

Each infrared channel of SEVIRI is analysed independently as they are processed independently in the inter-calibration products. Like the inter-calibration itself, this analysis is performed using radiances. However, the resulting uncertainties are presented here in terms of brightness temperature biases evaluated over the range of brightness temperatures observed in each SEVIRI channel, as it is believed that this allows easier interpretation of the results.

The full inter-calibration process is described in the ATBD [3]. However, the basic process is based on the selection of observations from the monitored instrument (Meteosat/SEVIRI) and the reference instrument (Metop/IASI) that are collocated in space, time and viewing geometry. The collocated observations are transformed to be comparable on spatial scale and spectral coverage and compared using a weighted regression. Each collocated observation is allocated a weighting based on its measure spatial variance and the specified radiometric noise of each channel. The regression propagates these variances to estimate the uncertainty on the corrected radiance, which provides a *Quality Indicator* for the inter-calibration product. However, these represent only two of many processes that introduce uncertainties to the final product, which make it prohibitive to conduct a full propagation of the uncertainties on each evaluation. So this document reviews the uncertainties through a *measurement model* of the process for case studies, which are assumed to represent typical conditions.

Because we have defined IASI as the reference for the inter-calibration, by definition any errors present in its data with respect to the truth should not be included in the uncertainty of

the inter-calibration products. However, some such terms have been included in this analysis to illustrate their magnitude (which is small). In these cases (which have been highlighted in the text), errors in the reference instrument have been interpreted as errors in the monitored instrument's observations.

Although the collocation criteria were designed to minimise any systematic errors by ensuring samples are symmetrically distributed, in reality small residual differences remain, which may introduce systematic errors in the end products. These sampling differences introduce errors in the radiances of each collocation, depending on their sensitivity to each variable, which is estimated using statistics from case studies. Where information is available on the sampling distribution, this has been used in the analysis – otherwise the collocation criteria have been taken as limits and propagated as standard uncertainties assuming the errors follow rectangular distributions within these limits. These are relatively simplistic treatments and it may be necessary to revise the estimates of one term if it becomes significant and a more accurate analysis is deemed necessary. This follows the approach recommended by ISO 14253-2, which defines an iterative procedure for uncertainty management (PUMA method). The decision of which uncertainty component needs to be improved is made on basis of the contribution of the components to the total uncertainty in the budget.

Similarly, different processes can introduce random errors on each collocated radiance. The magnitude of these can be estimated from the typical range of each variable and the sensitivity of the radiances to perturbation of each variable, which again can be derived from a statistical analysis of case study scenes. The regression process used to generate the GSICS Corrections reduces the impact of these random errors on each collocation and is repeated many times for randomly perturbed sets of collocations to estimate the resulting uncertainty on the corrected radiances due to each process in a *Monte Carlo*-like approach.

The collocation criteria represent trade-offs between the errors on each collocation and the number of collocations available. The uncertainty analysis presented here allows these trade-offs to be reviewed quantitatively to make recommendations to further improve the inter-calibration products.

2 GENERAL METHODOLOGY

For each process, typical differences in sampling variables between the monitored and reference instruments are estimated – either from the specified limits used to select the collocations (e.g. spatial sampling), or from the known differences (e.g. in sampling time). These differences are referred to as Δx in this document. The sensitivity of the radiances in each collocation to perturbations in each variable is also estimated. This is referred to as $\partial L/\partial x$ in this document.

The quantities input to the inter-calibration process are the radiances, L, of each collocation, i. In general, the uncertainty on L_i due to process j, is:

$$u_j(L_i) = \Delta x_{i,j}\left(\frac{\partial L}{\partial x}\right)_j, \qquad \textbf{Equation 1}$$

The GSICS Correction, $g(L)$, is based on the regression of collocated radiances observed by the monitored and reference instruments (Section 6.c of the ATBD [3]). It is a function which converts a radiance observed by the monitored instrument, L, to be consistent with the calibration of the reference, $\hat{L}$, which is the quantity output from the inter-calibration process:

$$\hat{L} = g(L). \qquad \textbf{Equation 2}$$

In GUM terminology $g(L)$ defines the *measurement model* of the inter-calibration process.

The observed radiances, L_i, are perturbed by $u(L_i)$. Then the regression is recalculated to generate a modified function, $g'(L)$, which will produce different corrected radiances, $\hat{L}'$:

$$\hat{L}' = g'(L_i + u(L_i)), \qquad \textbf{Equation 3}$$

This illustrates how errors in the collocated radiances can be propagated through to errors in the GSICS Correction applied to different scene radiances. These provide estimates of the uncertainty on the GSICS Correction, which are converted into brightness temperatures using the derivative of the Planck function evaluated at each scene radiance.

The uncertainties due to various mechanisms introducing systematic and random errors are analysed in the following sections based on case studies, using all the collocations used to produce the GSICS Re-Analysis Correction for Meteosat8/SEVIRI-MetopA/IASI on 2010-10-01.

Repeated evaluations with other cases show that the results of the combined uncertainty vary by a factor of ~ ±20%, depending on the distribution of collocated radiances used as input to the calculation of the GSICS Correction. However, this variability is much less than the variability of the evaluation of individual terms, which together limit the accuracy of this uncertainty analysis to a factor of ~2.

3 SYSTEMATIC ERRORS

3.1 Methodology for Systematic Errors

For processes introducing systematic errors, the radiance of each collocated point is perturbed by an amount representing its estimated uncertainty, $u^s_j(L_i)$,

$$u^s_j(L_i) = \Delta x^s_{i,j} \overline{\left(\frac{\partial L}{\partial x}\right)^s_j}, \qquad \textbf{Equation 4}$$

The regression used to calculate the GSICS Correction is recalculated, giving a modified function, $g'(L)$. This function is evaluated for a range of scene radiances and the resulting radiances compared to the corrected radiances generated by the unmodified function, $g(L)$ to provide an estimate of the uncertainty on the corrected radiance due to systematic errors introduced by process j:

$$u^s_j(\hat{L}) = \left| g'_j(L) - g_j(L) \right|, \qquad \textbf{Equation 5}$$

The modulo operation is necessary because the differences can have positive or negative sign.

Table 1 summarises the magnitude of typical perturbations, Δx_j, of processes introducing systematic errors in the collocated radiances and the sensitivity of the 8 infrared channels of SEVIRI to these perturbations, dL_j/dx. The origin of these values are discussed in the following sub-sections. Their implications are assessed in the summary of this section

Table 1 Summary of Systematic Errors' Perturbations and Sensitivities in RSS Mode

	Δx	Sensitivity, dLj/dx [mW/m2/st/cm-1/Δx]							
		IR03.9	IR06.2	IR07.3	IR08.7	IR09.7	IR10.8	IR12.0	IR13.4
Systematic Errors									
Temporal Mismatch	0.00278 hr	0.00814	0.09936	0.42332	1.21118	1.21931	2.05974	2.51872	2.39891
Longitudinal Mismatch	1.30639 km	-0.00001	0.00004	-0.00010	-0.00066	-0.00033	-0.00086	-0.00098	-0.00057
Latitudinal Mismatch	1.30639 km	0.00033	0.00203	0.00830	0.02743	0.02122	0.04516	0.05139	0.04214
Geometric Mismatch	-0.00847	0.00049	0.00864	0.03063	0.03461	0.10989	0.03737	0.04778	0.11284
Spectral Mismatch	1.00000	0.00014	0.00000	0.00000	0.00000	0.00000	0.00000	0.00000	0.00000
Spectral Calibration	0.50000	0.00009	0.00019	0.00025	0.00024	0.00029	0.00008	0.00009	0.00037

3.2 Temporal Mismatch

Systematic differences in the sampling time of the monitored and reference instruments can introduce systematic errors in their collocated radiances due to the diurnal cycle in the temperature, humidity, cloud and, hence, radiance emitted by the Earth's surface and atmosphere.

The selection of orbital data from the monitored and reference instruments are designed to select samples that are distributed with a uniform time difference over between the limits specified in the collocation criteria ($\pm\Delta t_{max}$=300 s in this case). For a GSICS Correction derived from $n \approx 30000$ collocations uniformly sampled over a period of $\pm\Delta t_{max}$, it would be expected that the mean time difference would have an uncertainty of $\Delta t = 2\Delta t_{max}/\sqrt{(3n)} \approx 2$ s. However, in practice deficiencies in the orbital selection cause the mean time difference to be Δt = 10 s (0.00278 hr).

The sensitivity of the radiances to changes in sampling time has been evaluated by calculating the mean difference between a large ensemble of radiances observed by Meteosat/SEVIRI in successive images. In this case, the mean difference between the nominal 21:30 and 21:35 images on 2010-07-29 over the target area domain of (35°W-35°E)x(15°N-35°N). The rate of change of radiance per hour for each infrared channel are shown in the first line of Table 1. However, these are not particularly reproducible and vary by a factor of ~2 on different days.

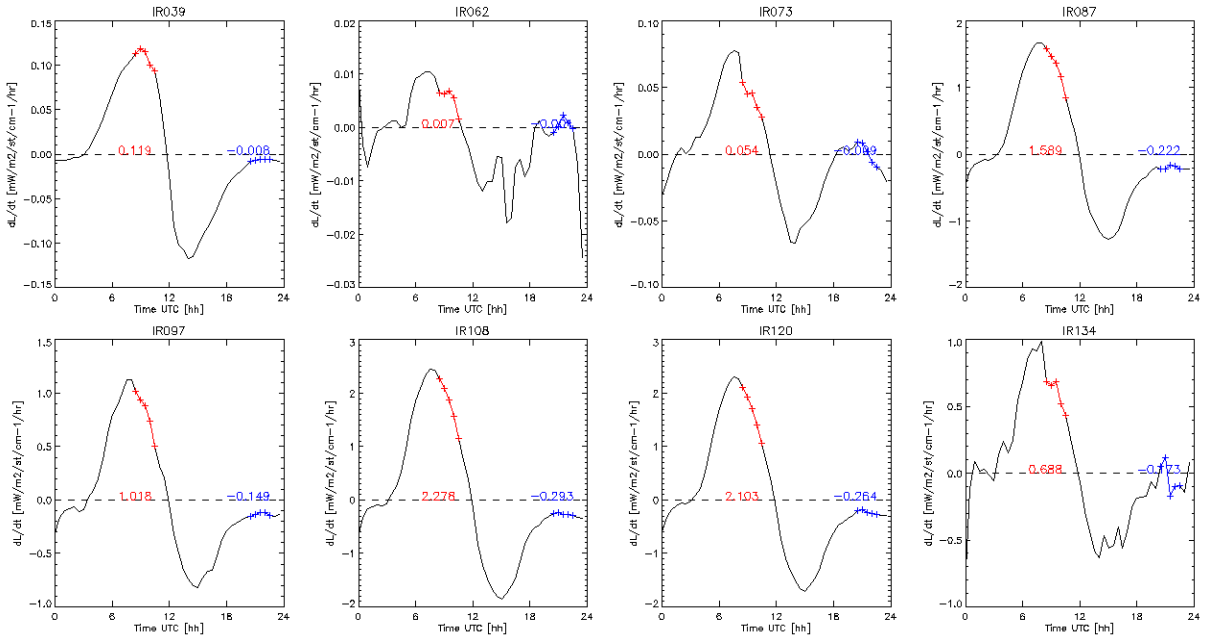

Figure 1 - Time series of mean rate of change of radiances calculated from Meteosat-9 observations on 2009-09-20 over (30°W-30°E)x(30°S-30°N).

Figure 1 shows the mean rate of change of radiances in each of the infrared channels of Meteosat-9 on 2009-09-20 over the target area domain. The period of the night-time overpass of Metop-A (~21:30) is highlighted in blue, showing the radiances are relatively stable at this time as the surfaces is gradually cooling. This contrasts with the period of the day-time

overpass (~09:30), when the surfaces are warming at close to their maximum rate. Using collocations from this period would increase the systematic uncertainty due to temporal mismatches by a factor of ~8 in most channels (except WV6.2). n.b. The diurnal cycle over the inter-calibration target domain covered in RSS mode is expected to be much larger, as it is dominated by the Sahara desert.

3.3 Longitudinal Mismatch

Systematic errors in the geolocation of both the monitored instrument (SEVIRI) and the reference instrument (IASI) being compared introduce errors in their collocated radiances due to small longitudinal mean gradients in their radiances over the domain of the collocations.

As the exact geolocation error on each pixel is not known, we assume they are distributed uniformly over the accuracies quoted for their navigation. The typical accuracy of the image navigation (rectification) for SEVIRI level 1.5 images based on the operational IMPF processing is calculated to be 1.2 km [4]. The geolocation accuracy of IASI level 1c data is calculated to be 1-2 km [5]. A value of 2 km is taken as a worst case limit – which may be refined later if this term is found to be dominant. These errors are assumed to be partitioned equally between longitude and latitude. Their uncertainties are combined linearly to act as a guard-band, so errors in longitudinal position are assumed to be distributed uniformly over $\pm\Delta lon_{max}=(1.2+2)/\sqrt{2}=2.26$ km. This is equivalent to a standard uncertainty of $\Delta lon=2.26/\sqrt{3}=1.30$ km.

The sensitivity of the collocated radiances to systematic errors in longitude was calculated as the mean difference in radiances between adjacent scan *elements* of a Meteosat-8 image over the RSS target domain, taken at 2010-07-29 21:30. These are shown in the second line of Table 1, expressed as radiance change per kilometre (after dividing the differences by the median pixel element separation, 3.41 km). Again, these are not particularly reproducible and vary by a factor of ~4 on different days.

3.4 Latitudinal Mismatch

Similarly, systematic errors in the geolocation of both instruments will introduce radiance errors due to larger latitudinal mean gradients over the domain of the collocations. Because navigation errors are assumed to be distributed equally between longitude and latitude, the combined uncertainty in the latitude of the collocations, $\Delta lat = \Delta lon = 1.30$ km, as above.

Similarly, the sensitivity of the collocated radiances to systematic errors in latitude was calculated as the mean difference in radiances between adjacent scan *lines* of a Meteosat-9 image over the target domain, taken at 2010-07-29 21:30. These are shown in the third line of Table 1, expressed as radiance change per kilometre (after dividing the differences by the median pixel line separation, 3.38 km). Again, these are not particularly reproducible and vary by a factor of ~4 on different days.

3.5 Geometric Mismatch

Collocations between different instruments on different satellites are never exactly aligned in terms of viewing and solar geometry. Although the radiances in the infrared channels of SEVIRI-IASI are not sensitive solar and azimuth angles during night-time conditions used in

this study, they are affected by the incidence angle – both in terms of absorption along different atmospheric paths and changes in surface emissivity.

Pixels are defined as collocations only if their incidence angles are such that the ratio of their atmospheric path difference is less than 5% (i.e. $|\Delta\sec\theta/\sec\theta|<0.05$). For a typical 30° incidence angle (over ±52°N/S GEO/LEO comparison domain), this corresponds to a difference of 5°. In practice collocations may have different incidence angles uniformly distributed within the range $\pm\Delta\theta = 5°$. However, if the actual distribution of viewing angles differences is not symmetrically distributed about zero, systematic biases will be introduced into the inter-calibration products. In this case we can use the actual differences in air mass ($\sec\theta$) calculated for the collocations used to calculate a typical GSICS Correction, which follow a rectangular distribution within the limits of $|\Delta\sec\theta/\sec\theta|<0.05$, with a mean value of $\Delta\sec\theta/\sec\theta=-0.008$.

A radiative transfer model (RTTOV9) was run for a diverse set of 77 atmospheric profiles in three cloud configurations (clear sky, uniform cloud with tops at 700 hPa and 300 hPa) to predict the radiances seen by the infrared channels of SEVIRI. This calculation was repeated at 30° and 29° incidence angles. The resulting sensitivities are shown in the fourth line of Table 1, expressed as radiance changes per degree of viewing zenith angle. These are equivalent to 0.02 K in the window channels to 0.11 K at IR9.7 when converted to brightness temperatures.

3.6 Spectral Mismatch

When radiances measured with non-identical channels are compared, great care must be taken to account for the differences introduced by their different spectral responses. Many methods have been developed to perform this *spectral correction*. However, no spectral correction method can be perfect and residual errors will remain in the compared radiances. Such errors can include systematic components, which introduce uncertainties that are not reduced by combining multiple comparisons.

Even using a hyperspectral reference instrument, such as IASI, there are uncertainties introduced in the comparison of collocated radiances with a broadband radiometer, such as SEVIRI. These errors can be due to hyperspectral instrument's spectral calibration accuracy and gap-filling methods used to account for its incomplete spectral coverage of the GEO channels. In theory, errors on the radiances observed by the reference instrument should not contribute to the uncertainty of the GSICS Correction to that reference. However, they are evaluated here to illustrate the likely magnitude of differences to the "true" scene radiance.

3.6.1 GEO-LEO Spectral Mismatch

Deficiencies in the hyperspectral LEO reference instrument's coverage of the broadband GEO instrument needs to be accounted for before their collocated observations can be compared. In general, the recommended approach is based on the *constrained optimization* gap filling described in [12].

However, in the case of SEVIRI-IASI inter-calibration a simplified approach can be adopted to account for this deficiency. Only SEVIRI's IR3.9 channel has incomplete coverage by IASI, which stops at 2760 cm^{-1}. A radiative transfer model (HITRAN) was used to calculate

radiance spectra over the full thermal infrared range for 9 atmospheres with different cloud amounts, following [12]. These were convolved with the SEVIRI SRFs and the integral over the full band compared with the integral of those truncated at 2760 cm^{-1}. A simple linear model was developed to estimate the radiance over the full SRF from that measured from the truncated SRF. This produced corrections ranging from -0.08 K to -0.35 K depending on the scene radiance. The r.m.s. uncertainty on the linear correction was 0.005 K – but only for the IR3.9 channel.

In general there will also be contributions from the systematic errors in the radiative transfer model used to perform the spectral correction when comparing the observations of two instruments. However, in the case of SEVIRI-IASI, the uncertainty in the gap filling correction is very small, so the modelling errors will have a negligible influence.

For consistency with the methods of assessing other components of the error budget, an uncertainty of $\Delta=1$ (dimensionless) has been assigned to the gap-filling correction and the sensitivity of the collocated radiances has been estimated as above in the fifth line of Table 1.

n.b. For AIRS this term will dominate the uncertainty budget. Its magnitude may be estimated by evaluating the maximum/minimum contours of the residuals of the gap-filling validation, as plotted in Figures 21-28(f) of TR52 [12].

3.6.2 LEO Spectral Calibration Accuracy

The relative spectral calibration accuracy of IASI is estimated to be $\Delta\nu/\nu=0.5$ ppm [10]. The sensitivity of the collocations' radiances to systematic shifts in the centre frequency of IASI's channels has been estimated by shifting the wavenumbers of the SRFs by this ratio and repeating the spectral convolution. These are shown in the sixth line of Table 1 in terms of radiance change per ppm frequency shift.

The resulting radiances are negligibly different from those calculated for the unperturbed SEVIRI channels. Even when using a shift of 2 ppm, corresponding to IASI's specified maximum relative spectral calibration accuracy [11], the rms difference in brightness temperature is <1 mK for all channels.

3.6.3 GEO Spectral Response Function Interpolation

The official SRF of SEVIRI's channels is calculated from a series of tests performed on its component parts. These are combined and expressed at irregular wavelength intervals defined to represent the full SRF with minimal errors. However, the SRF definitions are open to interpretation, which may introduce errors in the radiances when compared to a hyperspectral reference instrument. For example, although it is recommended that a linear interpolation is used to convert the published SRFs to the IASI channel wavenumbers, it is possible to use other interpolation methods. The calculations were repeated using linear and quadratic interpolation and the results compared to estimate the magnitude of likely errors introduced due to this ambiguity. This term is quite small (<~0.01 K), and has been neglected in this analysis as we assume the SRFs are interpreted as recommended and consistently between the application of the GEO observations and in the calculation of the inter-calibration. This highlights the importance of communicating clear guidance in the application of published SRFs.

3.7 Combining and Comparing all Systematic Errors

All the uncertainties due to systematic processes, are added in quadrature to give $u^s(L)$:

$$u^s(L) = \left\{ \sum_j \left(u_j^s(L) \right)^2 \right\}^{1/2}, \qquad \textbf{Equation 6}$$

This total uncertainty on the corrected radiance due to all systematic errors is compared with the contribution from each considered mechanism in Figure 2. Here the uncertainties have been evaluated for the range of radiances observed over all the collocations used in the sample case. The radiances and uncertainties are converted to brightness temperatures for convenient comparison.

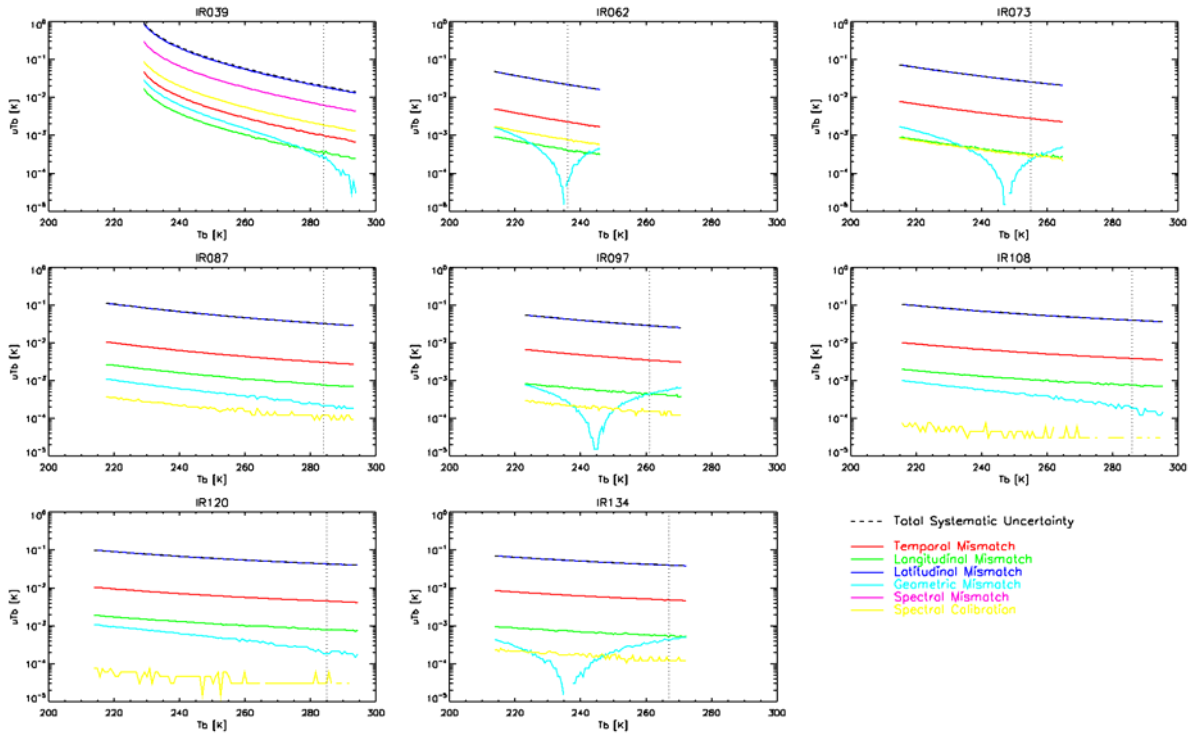

Figure 2 – Contribution of each source of Systematic Error to the Uncertainty of the Brightness Temperatures (Tb) produced by the GSICS Correction for a range of scene radiances for each infrared channel of RSS mode Meteosat8/SEVIRI using MetopA/IASI reference. Dotted vertical line shows standard scene radiance for each channel.

Figure 2 shows that the latitudinal systematic mismatches dominate the total systematic uncertainty due to north-south gradients in the scene over the inter-calibration target domain. However, the systematic errors in the IR3.9 channel are also influenced by the uncertainty in the spectral correction method applied to compensate for the incomplete coverage of this channel by IASI. Other terms due to temporal and geometric mismatches and the spectral calibration of the reference instrument are negligible in all cases and the latter appear erratic due to the limitations of numerical precision.

Table 2 Systematic Error Budget of GSICS Correction for SEVIRI-IASI Standard Scenes based on Meteosat8/SEVIRI in Rapid Scan Service (RSS) Mode

Meteosat SEVIRI Channel	IR03.9	IR06.2	IR07.3	IR08.7	IR09.7	IR10.8	IR12.0	IR13.4	
Standard Scene Radiance	284	236	255	284	261	286	285	267	K
Temporal Mismatch	0.0010	0.0023	0.0028	0.0031	0.0035	0.0039	0.0045	0.0048	K
Longitudinal Mismatch	-0.0003	0.0004	-0.0003	-0.0008	-0.0005	-0.0007	-0.0008	-0.0005	K
Latitudinal Mismatch	0.0191	0.0218	0.0257	0.0325	0.0287	0.0398	0.0431	0.0399	K
Geometric Mismatch	-0.0002	0.0000	-0.0002	-0.0002	-0.0005	-0.0002	-0.0002	-0.0004	K
Spectral Mismatch	0.0063	0.0000	0.0000	0.0000	0.0000	0.0000	0.0000	0.0000	K
Spectral Calibration	0.0019	0.0008	0.0003	0.0001	0.0002	0.0000	0.0000	0.0001	K
Total Systematic Uncertainty	0.0202	0.0220	0.0259	0.0326	0.0289	0.0400	0.0433	0.0402	K

Table 2 shows the uncertainties in the GSICS Correction evaluated at standard scene radiances due to systematic errors in each of the six mechanism considered. These uncertainties are expressed in brightness temperatures for each of the 8 infrared channels of SEVIRI, based on only night-time collocation data within the target area domain for the collocations (35°W-35°E)x(15°N-35°N). The last row shows the total systematic uncertainty (unexpanded k=1), due to all terms combined following equation (6).

4 RANDOM ERRORS

4.1 Methodology for Random Errors

A Monte-Carlo approach is adopted to evaluate the uncertainty on the final correction for processes which introduce random errors. The radiance of each collocated point is perturbed by an uncertainty calculated by multiplying a random number, z_i, drawn from a distribution consistent with a characteristic difference, Δx^r, multiplied by the sensitivity to random perturbations of this process, $(\partial L/\partial x)^r_j$ as follows:

$$u^r_j(L_i) = \overline{\Delta x^r_j} z_i \overline{\left(\frac{\partial L}{\partial x}\right)^r_j}, \qquad \textbf{Equation 7}$$

The regression used to calculate the GSICS Correction is then re-evaluated with one set of randomly perturbed radiances. The resulting regression coefficients are used to evaluate the radiances bias over a range of scene radiances. This procedure is then repeated a large number (n_k) of times to give n_k evaluations of $g'_{j,k}(L)$. Each evaluation of which is used to calculate a corrected radiance for each of a range of scene radiances, $\hat{L}'_{j,k}$.

The standard deviation of $\hat{L}'_{j,k}$ over the Monte Carlo ensemble is then calculated to provide an estimate of the uncertainty on corrected radiances due to each random process, j:

$$u^r_j\left(\hat{L}\right) = \left\{ \sum_{k=1}^{n} \frac{\left(g'_{j,k}(L)\right)^2}{n_k(n_k-1)} - \sum_{k=1}^{n} \left(\frac{g'_{j,k}(L)}{n_k(n_k-1)} \right)^2 \right\}^{1/2}, \qquad \textbf{Equation 8}$$

Table 3 summarises the magnitude of typical perturbations, Δx_j, of processes introducing random errors in the collocated radiances and their sensitivity to these perturbations, dL_j/dx. The origin of these values are discussed in the following sub-sections. Their implications are assessed in the summary of this section.

Table 3 Summary of Random Errors' Perturbations and Sensitivities in RSS Mode

	Δx	Sensitivity, dLj/dx [mW/m2/st/cm-1/Δx]							
		IR03.9	IR06.2	IR07.3	IR08.7	IR09.7	IR10.8	IR12.0	IR13.4
Random Errors									
Temporal Variability	5.00 min	0.00575	0.02123	0.09666	0.39062	0.32717	0.64751	0.72228	0.57434
Longitudinal Variability	3.41 km	0.00511	0.00663	0.03690	0.26396	0.16885	0.40084	0.42600	0.24139
Latitudinal Variability	3.38 km	0.00668	0.01954	0.08928	0.40672	0.31711	0.65604	0.72155	0.53597
Geometric Variability	5.00	0.00049	0.00864	0.03063	0.03461	0.10989	0.03737	0.04778	0.11284
Spectral Variability	1.00	0.00014	0.00000	0.00000	0.00000	0.00000	0.00000	0.00000	0.00000
Radiometric Noise (GEO)	1.00	0.00054	0.00172	0.00587	0.02545	0.02807	0.03265	0.04823	0.09398
Radiometric Noise (LEO)	1.00	0.00076	0.00122	0.00210	0.02874	0.02906	0.02369	0.02798	0.02489

4.2 Temporal Variability

Collocated observations from a pair of satellite instruments are not sampled simultaneously. Variations in the atmosphere and surface during the interval between their observations introduce errors when comparing their collocated radiances. The greater this interval, the larger the contribution of the scene's temporal variability to the total error budget. The uncertainty this introduces to the collocated radiances can be quantified by statistical analysis of a series of SEVIRI scenes described below.

GEO imagers sample scenes at regular intervals: SEVIRI can scan the whole Earth disk every 15 min, or one third of it every 5 min in rapid scan mode. The latter corresponds to the maximum interval recommended in the ATBD for its pixels to be considered collocated with those of IASI. This finite sampling introduces a temporal collocation error with a uniform distribution over $\pm\Delta t_{max}$= 300 s. This is equivalent to an r.m.s. difference between sampling of SEVIRI and IASI observations of $\Delta t = \Delta t_{max} / \sqrt{3} \approx 173$ s.

The temporal variability of typical SEVIRI images was originally quantified for each infrared channel in [6]. The root mean squared difference (RMSD) between the channels' radiances was calculated after shifting the images sampled in rapid scanning mode by various intervals. As seen in Figure 3 (Figure 1 of [6]), the RMSD was found to increase approximately linearly with interval for closely separated time intervals.

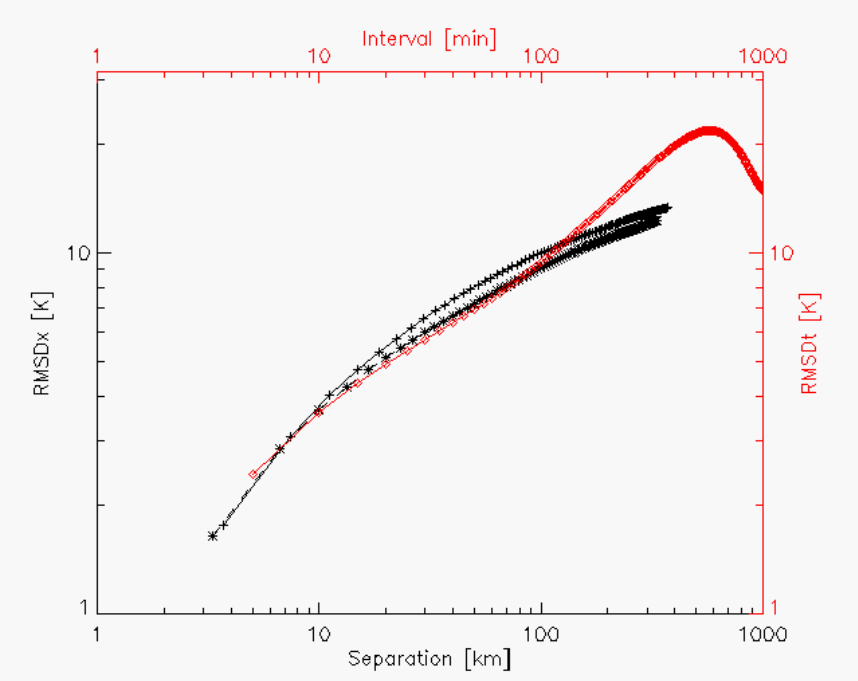

Figure 3 R.M.S. differences in Meteosat-8 10.8 µm brightness temperatures with time intervals from Rapid Scanning Meteosat data (red diamonds) and with spatial separation in North-South direction (black pluses) and West-East direction (black red stars) [6].

In this analysis the sensitivity of the radiances to differences in sampling time has been evaluated by calculating the RMSD between a large ensemble of radiances observed by Meteosat/SEVIRI in successive images. In this case, we calculate the RMSD between the nominal 21:30 and 21:35 images on 2010-07-29 over the target area domain covered in RSS

mode (35°W-35°E)x(15°N-35°N). To best reproduce the data used in the inter-calibration, the SEVIRI images are first smoothed by applying a 5x5 smoothing window. The RMSD for each infrared channel are shown in the first line of Table 3, expressed as a rate of change of radiance per minute.

4.3 Longitudinal Variability

Similarly, collocated observations from a pair of satellite instruments are not exactly collocated and spatial variations in the atmosphere and surface introduce errors when comparing their collocated radiances. The greater the separation between their observations, the larger the contribution of the scene's spatial variability to the total error budget. The uncertainty this introduces to the collocated radiances can be quantified by statistical analysis of a representative SEVIRI scenes described below.

SEVIRI's level 1.5 data has been re-projected onto a grid, with approximately uniform spacing near the sub-satellite point and over the target domain of the collocations in RSS mode (35°W-35°E)x(15°N-35°N), where the median distance between adjacent pixel elements in 3.41 km. It is assumed that the difference longitude between *collocated* radiances measured by SEVIRI and IASI follows a uniform distribution over $\pm\Delta lon_{max}$ = 3.41 km.

The spatial variability of a typical SEVIRI image was also quantified for each infrared channel in [6]. The root mean squared difference (RMSD) between the channels' radiances was calculated after shifting the images by various latitude and longitude offsets. As seen in Figure 3 (Figure 1 of [6]), the RMSD was found to increase approximately linearly with interval for closely separated spatial intervals.

In this analysis the sensitivity of the radiances to differences in sampling longitude has been evaluated by calculating the RMSD between all radiances observed by Meteosat/SEVIRI in adjacent pixel elements. In this case, the 21:30 images on 2010-07-29 covering the RSS mode target area domain of (35°W-35°E)x(15°N-35°N) was analysed after first applying a 5x5 smoothing window to represent the spatial averaging that is done in the inter-calibration. The RMSD for each infrared channel are shown in the second line of Table 3, expressed as a rate of change of radiance per kilometre (after dividing the differences by the median pixel element separation, 3.41 km).

4.4 Latitudinal Variability

The same methodology is applied to quantify the collocated radiances' sensitivity to errors in latitude as the RMSD between adjacent scan lines of the same smoothed SEVIRI image, using a median scan line separation of 3.38 km. The results are shown in the third line of Table 3.

4.5 Geometric Variability

Random differences between the viewing and solar geometry of the collocations observed by the monitored and reference instruments also introduce random errors to their collocated radiances. Although the infrared radiances are not sensitive to solar and azimuth angles during night-time conditions used in this study, they are affected by the incidence angle –

both in terms of absorption along different atmospheric paths and changes in surface emissivity.

As in the case of systematic geometric mismatches (§3.5), the differences in viewing zenith angle between the two sensors is uniformly distributed within the range $\pm\Delta\theta = 1°$, corresponding to a <1% difference in *air mass*. Likewise, the sensitivity of the collocated radiances to viewing zenith angle is the same as for systematic geometric mismatches, as shown in the fourth line of Table 3.

4.6 Spectral Variability

The spectral calibration accuracy of IASI discussed in §3.6.2 is assumed to also introduce random errors to the collocated radiances, following a normal distribution with $\Delta\nu/\nu$=0.5 ppm and the same sensitivity evaluated in §3.6.2, as shown in the fifth line of Table 3.

4.7 Radiometric Noise

All radiometer observations suffer from radiometric noise caused by limitations of the instruments. This noise contributes to the uncertainty in the comparison of collocated observations. However, the impact of radiometric noise can be reduced by averaging multiple observations, spatially, temporally and spectrally.

The contributions of radiometric noise to the collocated radiances of both GEO and LEO instruments is quantified in Table 4 in terms of brightness temperatures, and summarised in Table 3 in radiance units with Δ=1, following a normal distribution. However, these terms are implicitly included in both the spatial and temporal variability terms as they are calculated using real observational data, which is subject to radiometric errors. It is, therefore, reassuring to see these terms have negligible contributions to the overall uncertainties. So although they have been double-counted in the error budget, this does not matter as their contributions are insignificant compared to the temporal and spatial variability of the scene.

4.7.1 GEO Radiometric Noise

Typical radiometric noise on SEVIRI level 1.5 radiances is given in [7]. The mean value of the range of observed noise measurements (NEΔT) given in Table 4 of [7] for ambient scenes with the instrument at 95K are used here, which are well within the specified limits.

Although the radiances from 5x5 arrays of SEVIRI pixels are averaged, there is considerable over-sampling in the rectified level 1.5 image data used. This results in the 25 GEO pixels not being independent, so the variance calculated from the level 1.5 data should be reduced by an *oversampling factor* to estimate the true scene variance. For each GEO channel an *effective Field of View* (FoV) can be estimated from the spatial frequencies at which the published Modulation Transfer Functions [8] drop to 50% in the N-S and E-W planes (~0.11 km^{-1}). The geometric average of these effective FoVs (~4.5 km) is compared with the sampling interval of the level 1.5 image (3.0 km near the sub-satellite point) to give the oversampling factor (~1.5). The actual number of GEO pixels (25) is reduced by this factor squared to estimate the effective number of GEO pixels (~11). The radiometric uncertainty of the mean radiance of the GEO pixels is, therefore, reduced by the square root of this oversampling factor (~$\sqrt{11}$) relative to the nominal values for SEVIRI's radiometric noise given in [7].

4.7.2 LEO Radiometric Noise

The radiometric noise on each IASI spectral sample within SEVIRI's passbands is estimated from Figure 1 of [9]. When expressed in brightness temperatures these range from 0.1 K for the IR7.3 channel to 1.3 K for the IR3.9 channel. After convolution with the SRF of the SEVIRI channels, this is reduced by the square root of a factor referred to here as the *effective number of LEO channels*, which is estimated as the integral of the normalised SRFs sampled at the spectral interval of the IASI channels. This factor ranges from 1452 for the broadest IR3.9 channel to 272 for the narrowest IR13.4 channel. The effective LEO radiometric noise is evaluated as the mean radiometric noise on the constituent channels divided by the square root of the effective number of LEO channels.

Table 4 Contributions from Radiometric Noise to Collocations' Radiances

Central Wavelength	3.9	6.2	7.3	8.7	9.7	10.8	12.0	13.4	µm
Radiometric Noise GEO	0.09	0.05	0.05	0.08	0.10	0.07	0.10	0.21	K
Number of GEO pixels/LEO FoV	25	25	25	25	25	25	25	25	
Spatial Freq for MTF=0.5 EW	0.125	0.121	0.117	0.113	0.113	0.109	0.107	0.100	/km
Spatial Freq for MTF=0.5 NS	0.121	0.121	0.117	0.109	0.113	0.105	0.105	0.100	/km
Effective FoV	4.1	4.1	4.3	4.5	4.4	4.7	4.7	5.0	km
GEO Sampling Dist @ SSP	3	3	3	3	3	3	3	3	km
Oversampling factor	1.4	1.4	1.4	1.5	1.5	1.6	1.6	1.7	
Effective number GEO channels /Collocation	1	1	1	1	1	1	1	1	
Effective number of GEO pixels /Collocation	14	13	12	11	11	10	10	9	
Radiometric Noise <GEO>	0.024	0.014	0.014	0.023	0.029	0.022	0.031	0.068	K
Wavenumber	2564	1613	1370	1149	1031	926	833	746	cm-1
Radiometric Noise LEO	1.30	0.30	0.10	0.35	0.30	0.30	0.30	0.30	K
Effective number LEO channels	1452	867	345	181	103	348	276	272	
Effective number of LEO pixels /Collocation	1	1	1	1	1	1	1	1	
Radiometric Noise <LEO>	0.034	0.010	0.005	0.026	0.030	0.016	0.018	0.018	K

4.8 Combining and Comparing all Random Errors

All the uncertainties due to random processes, are added in quadrature to give $u^r(L)$:

$$u^r(L) = \left\{ \sum_j \left(u_j^r(L) \right)^2 \right\}^{1/2}, \qquad \textbf{Equation 9}$$

This total uncertainty on the corrected radiance due to all random errors is compared with the contribution from each considered mechanism in Figure 4. Here the uncertainties have been

evaluated for the range of radiances observed over all the collocations. The radiances and their uncertainties are converted to brightness temperatures for convenient comparison.

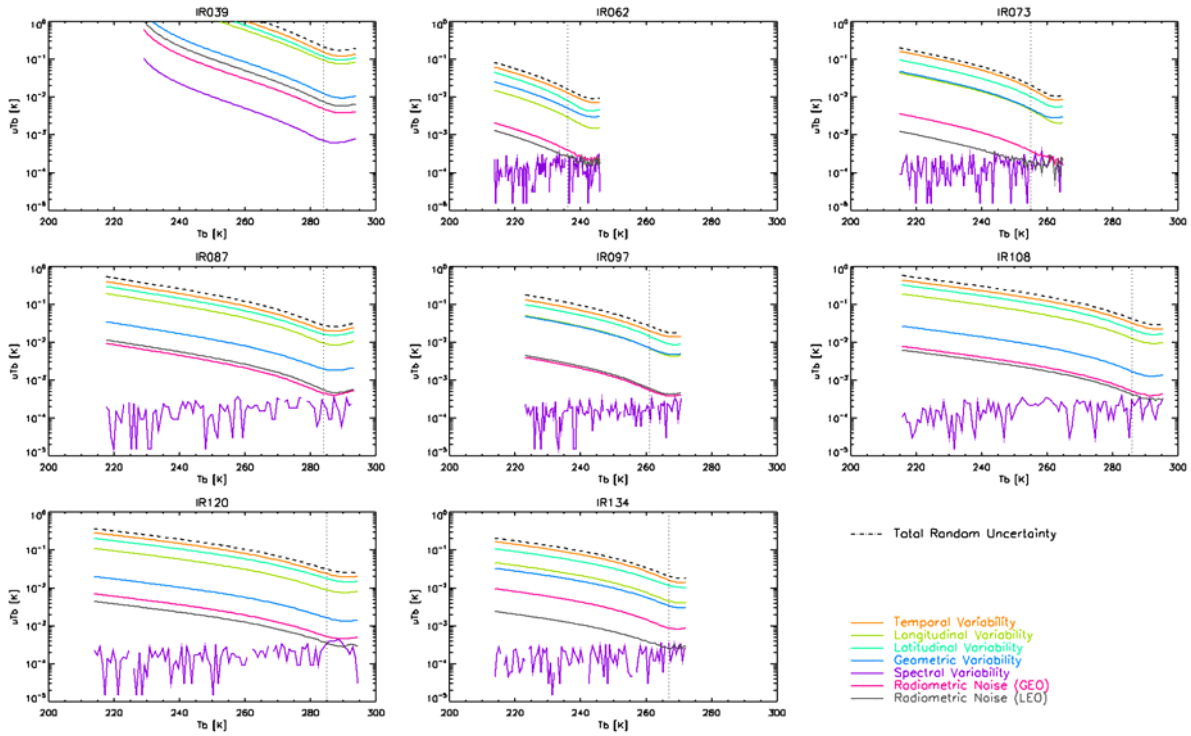

Figure 4 – Contribution of each source of Random Error to the Uncertainty of the Brightness Temperatures (Tb) produced by the GSICS Correction for a range of scene radiances for each infrared channel of RSS mode Meteosat8/SEVIRI using MetopA/IASI reference. Dotted vertical line shows standard scene radiance for each channel.

Figure 4 shows that the random variability in time and space dominate the total random uncertainty in all channels. Other terms due to geometric and spectral variability are negligible in all cases and the latter appear erratic due to the limitations of numerical precision. It is also reassuring to find that the contribution from the radiometric noise of both instruments is also negligible, as this terms are implicitly included in the evaluation of the spatial and temporal variability.

These results suggest the time limit of $|\Delta t| < 300$ s specified in the collocation criteria is well matched to the spatial variability due to SEVIRI's 3 km sampling. Furthermore, it suggests that the relaxation of the specified collocation criteria for the difference of viewing zenith angle $|\Delta \sec\theta / \sec\theta| < 0.05$ recommended in the previous analysis [EUM/MET/TEN/09/0750] has not caused a significant increase in the overall uncertainty of the inter-calibration result. Only in the water vapour channels does this term now become comparable to the contribution due to longitudinal variability.

Table 5 shows the uncertainties in the GSICS Correction evaluated at standard scene radiances due to random errors in each of the seven mechanism considered. These uncertainties are expressed in brightness temperatures for each of the 8 infrared channels of SEVIRI, based on only night-time collocation data within the RSS mode target area domain

for the collocations (35°W-35°E)x(15°N-35°N). The last row shows the total random uncertainty (unexpanded k=1), due to all terms combined following equation (6).

Table 5 Random Error Budget of GSICS Correction for SEVIRI-IASI at Standard Scene

Meteosat SEVIRI Channel	IR03.9	IR06.2	IR07.3	IR08.7	IR09.7	IR10.8	IR12.0	IR13.4	
Standard Scene Radiance	284	236	255	284	261	286	285	267	K
Temporal Variability	0.1567	0.0130	0.0168	0.0213	0.0203	0.0328	0.0240	0.0163	K
Longitudinal Variability	0.0955	0.0030	0.0046	0.0095	0.0071	0.0128	0.0090	0.0046	K
Latitudinal Variability	0.1196	0.0081	0.0104	0.0165	0.0145	0.0221	0.0180	0.0118	K
Geometric Variability	0.0125	0.0051	0.0049	0.0020	0.0072	0.0017	0.0016	0.0035	K
Spectral Variability	0.0007	0.0000	0.0000	0.0000	0.0000	0.0000	0.0000	0.0000	K
Radiometric Noise (GEO)	0.0049	0.0004	0.0004	0.0004	0.0006	0.0005	0.0005	0.0009	K
Radiometric Noise (LEO)	0.0076	0.0002	0.0001	0.0006	0.0006	0.0004	0.0004	0.0003	K
Total Random Uncertainty	0.2196	0.0164	0.0209	0.0286	0.0270	0.0416	0.0314	0.0209	K

Although the mean time difference between the SEVIRI and IASI observations in rapid scanning mode is much reduced compared to full disc scanning, there is much larger temporal variability of the scene in the target area of the collocations, which is dominated by the Sahara desert. This results in a larger contribution from temporal variability. There is also a strong contribution due to north-south gradients in this area.

4.9 Validation of Quoted Uncertainty on GSICS Correction

Table 6 compares the total uncertainty due to random errors predicted by this analysis with the median value of the uncertainty quoted within the GSICS Re-Analysis products for SEVIRI-IASI. This shows the regression used in the ATBD tends to under-estimate the uncertainties by a factor of 3 – 12 for channels IR6.2-IR13.4 (the mean ratio is 6.4). However, the IR3.9 uncertainty is underestimated by a factor of 64!

Table 6 Validation of GSICS Correction for SEVIRI-IASI Error Budget

Meteosat SEVIRI Channel	IR03.9	IR06.2	IR07.3	IR08.7	IR09.7	IR10.8	IR12.0	IR13.4	
Standard Scene Radiance	284	236	255	284	261	286	285	267	K
Typical Standard Correction	0.309	-0.140	0.544	0.035	0.026	0.010	0.040	-0.209	K
Total Random Uncertainty	0.220	0.016	0.021	0.029	0.027	0.042	0.031	0.021	K
Median Uncertainty Quoted	0.004	0.005	0.005	0.003	0.004	0.003	0.005	0.005	K
Rolling SD of Standard Bias	0.031	0.017	0.015	0.008	0.013	0.008	0.011	0.009	K

4.10 Comparison of Theory with Statistics

Table 6 also compares the results of this analysis with the day-to-day variability observed in the biases estimated for standard radiance scenes by GSICS Re-Analysis Correction. This is

calculated as the standard deviation evaluated over 15 day rolling windows. These show the variability of the GSICS Correction is comparable to the theoretical random uncertainty from this analysis for most channels. However, it suggests that the uncertainty for the IR3.9 channel is over-estimated by a large factor in this analysis. It is, therefore, recommended that the quoted uncertainties are inflated by a factor of 6.4 to account for additional contribution to the uncertainty which are not accounted for in the regression analysis used to generate the GSICS Correction.

Unsurprisingly these analytical values are larger than the analysis of Meteosat9/SEVIRI operating in full disc scanning mode. However, they are no longer much smaller than the day-to-day variability of the standard biases, suggesting the method of calculating the GSICS Correction is no longer 'better' than the instrument's stability.

5 COMBINING SYSTEMATIC AND RANDOM ERRORS

5.1 Method for Combining Systematic and Random Errors

The total uncertainties due to systematic and random processes can then be combined to give the total combined uncertainty, u^c, for a given radiance, L:

$$u^c(L) = \left\{ \left[u^s(L)\right]^2 + \left[u^r(L)\right]^2 \right\}^{1/2}. \qquad \textbf{Equation 10}$$

Figure 5 compares the impact of all the systematic and random errors on the uncertainty of the GSICS Correction evaluated over a range of radiances. This shows that in most conditions the random components of the uncertainty dominate for all channels. It also shows that the uncertainties increase rapidly for low radiance scenes, and reach a minimum near the standard radiances for each channel. This is because the majority of the collocations give radiances near these values, whereas cold, high clouds are relatively infrequent. It is also clear that the GSICS Correction produces much smaller uncertainties in channels with stronger atmospheric absorption, as the scenes are inherently less variable.

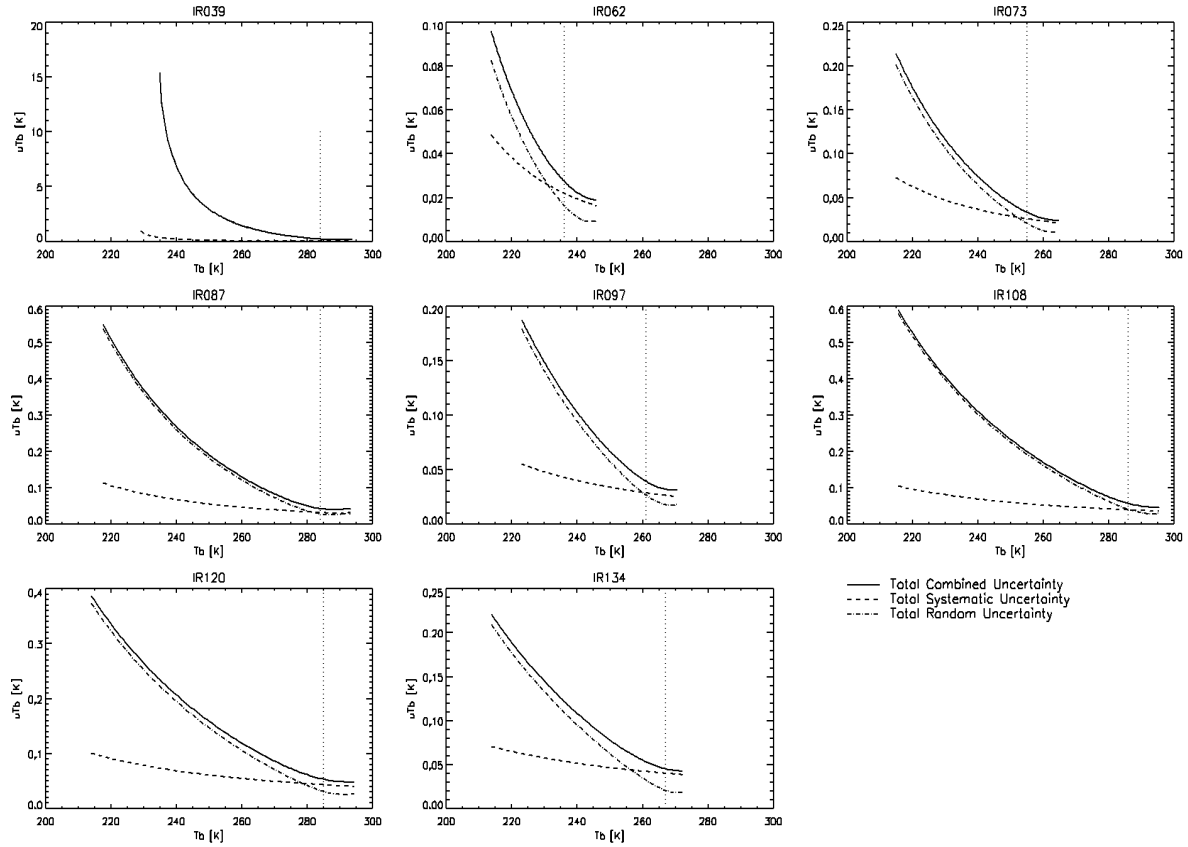

Figure 5 – Impact of Total Systematic and Random Errors on Uncertainty of the Brightness Temperatures (Tb) produced by the GSICS Correction for a range of scene radiances for each infrared channel of RSS mode Meteosat8/SEVIRI using MetopA/IASI reference. Dotted vertical line shows standard scene radiance for each channel.

Table 7 Overall Error Budget of GSICS Correction for SEVIRI-IASI for Standard Scenes

Meteosat SEVIRI Channel	IR03.9	IR06.2	IR07.3	IR08.7	IR09.7	IR10.8	IR12.0	IR13.4	
Standard Scene Radiance	284	236	255	284	261	286	285	267	K
Typical Standard Correction	0.309	-0.140	0.544	0.035	0.026	0.010	0.040	-0.209	K
Total Systematic Uncertainty	0.020	0.022	0.026	0.033	0.029	0.040	0.043	0.040	K
Total Random Uncertainty	0.220	0.016	0.021	0.029	0.027	0.042	0.031	0.021	K
Total Combined Uncertainty	0.221	0.027	0.033	0.043	0.040	0.058	0.054	0.045	K

Table 7 shows the systematic, random and combined uncertainties of the GSICS Re-Analysis Correction for standard radiance scenes. These values are generally small, with total combined uncertainties ~40 mK. (Although the total uncertainties are much larger for the IR3.9 channel, as noted previously this is believed to be partly due to an over-estimation due to the this channel's random variability of the sample scenes used in this analysis.)

The total combined uncertainty can be compared to typical levels of the correction for each channel, which are generally an order of magnitude larger. This shows that, although the corrections may be small for most channels, they are statistically significant at the 95% confidence level for the water vapour and IR13.4 channels.

6 RECOMMENDATIONS

This analysis has evaluated the uncertainties for the GSICS Re-Analysis Correction of Meteosat/SEVIRI using Metop/IASI as a reference, with Meteosat operating in rapid scanning service (RSS) mode. Random errors on the Near Real-Time corrections would be approximately √2 larger due to approximately half the number of collocations being used in the regression. Systematic errors would remain unchanged.

This analysis validates the approach and collocation thresholds used in the inter-calibration of the infrared channels of SEVIRI-IASI. In particular, it suggests that the relaxation of the specified collocation criteria for the difference of viewing zenith angle $|\Delta\sec\theta/\sec\theta|<0.05$ recommended in the previous analysis [EUM/MET/TEN/09/0750] has not caused a significant increase in the overall uncertainty of the inter-calibration result. It also shows that the temporal limit of 300 s should not be relaxed as this would increase the uncertainty of the final GSICS Correction.

Ideally, the ATBD should be revised to account for correlations within the data when estimating the uncertainty on the GSICS Correction, following this analysis. Alternatively, the uncertainty estimated from the weighted regression in the ATBD should be inflated empirically by a factor of ~6.4 to achieve greater consistency between the statistics of the GSICS Correction and this analysis. However, this should be reviewed once statistics from the pre-operational product become available.

This analysis does not include contributions associated with the interpretation of the SRFs published for the GEO imager, as explained in §3.6.3. If included, this term could dominate the systematic errors of most channels. This highlights the importance of communicating clear guidance in the application of published SRFs.

Although some of these conclusions can be generalised to other pairs of GEO-LEO hyperspectral infrared inter-calibrations, the analysis should be repeated for each inter-calibration pair. Particular attention should be paid to the analysis of any gap-filling methods used in spectral corrections, which could dominate the uncertainties for other inter-calibrations. The analysis should also be repeated following any substantial changes to the ATBD.

REFERENCES

1. Nigel Fox, 2010: *A guide to expression of uncertainty of measurements*, QA4EO Guideline QA4EO-QAEO-GEN-DQK-006.
2. JCGM 2008: *Evaluation of measurement data – Guide to the expression of uncertainty in measurement*, http://www.bipm.org/en/publications/guides/gum.html
3. Tim Hewison, 2010: *ATBD for EUMETSAT's Inter-Calibration of SEVIRI-IASI*, EUM/MET/REP/08/0468.
4. EUMETSAT, 2007: *Typical Geometrical Accuracy for MSG-1/2*, EUM/OPS/TEN/07/0313.
5. IASI L1 Cal/Val Team, 2007: *Presentation of the IASI Level 1 Cal/Val Results*, 23/10/2007, EUMETSAT, Darmstadt
6. Tim Hewison, 2009: *Quantifying the Impact of Scene Variability on Inter-Calibration*, GSICS Quarterly, Vol. 3, No. 2.
7. EUMETSAT, 2007: *Typical Radiometric Accuracy and Noise for MSG-1/2*, EUM/OPS/TEN/07/0314.
8. EUMETSAT, 2006: *MSG-2 SEVIRI Modulation Transfer Function Characterisation*, EUM/MSG/TEN/06/0010.
9. Denis Blumstein, 2007: *In-flight performance of the infrared atmospheric sounding interferometer (IASI) on Metop-A*, Proc. of SPIE, Vol. 6684, 66840H-1, doi: 10.1117/12.734162.
10. B. Tournier and Co-Authors, 2007: *IASI on MetOp-A – Radiometric and spectral performances measured during commissioning*. First IASI Conference, Anglet, France, 13-16 November 2007, http://smsc.cnes.fr/IASI.
11. Denis Blumstein, 2008: *MetOp-A IASI Level 1 Cal/Val at IASI TEC*, GSICS Quarterly, Vol. 2, No. 2, 2008.
12. Tahara, Yoshihiko and Koji Kato, 2009: *New Spectral Compensation Method for Intercalibration Using High Spectral Resolution Sounder*, JMA Meteorological Satellite Center Technical Note No. 52, 1-37.